SCIENCE CHINA
Technological Sciences

•Article•

December 2023 Vol.66 No.12: 3462–3474
https://doi.org/10.1007/s11431-023-2496-6

Machinery fault diagnostic method based on numerical simulation driving partial transfer learning

LOU YunXia, KUMAR Anil & XIANG JiaWei*

College of Mechanical and Electrical Engineering, Wenzhou University, Wenzhou 325035, China

Received April 22, 2023; accepted August 30, 2023; published online November 16, 2023

Artificial intelligence (AI), which has recently gained popularity, is being extensively employed in modern fault diagnostic research to preserve the reliability and productivity of machines. The effectiveness of AI is influenced by the quality of the labeled training data. However, in engineering scenarios, available data on mechanical equipment are scarce, and collecting massive amounts of well-annotated fault data to train AI models is expensive and difficult. In response to the inadequacy of training samples, a numerical simulation-based partial transfer learning method for machinery fault diagnosis is proposed. First, a suitable simulation model of critical components in a mechanical system is developed using the finite element method (FEM), and numerical simulation is performed to acquire FEM simulation samples containing different fault types. Second, several synthetic simulation samples are generated to form complete source domain training samples using a generative adversarial network. Subsequently, the partial transfer learning network is trained to extract shared fault characteristics between the simulation and measured samples in the case of class imbalance. Finally, the resulting model is used to diagnose unknown samples from real-world mechanical systems in operation. The proposed method is tested on actual fault samples of bearings and gears obtained from a public dataset and experimental test rig available in our laboratory, achieving average classification accuracy of 99.54% and 99.64%, respectively. Comparison investigations reveal that the proposed method has superior classification and generalization ability when detecting faults in real mechanical systems.

finite element method, generative adversarial network, fault diagnosis, partial transfer learning, bearing, gear

Citation: Lou Y X, Kumar A, Xiang J W. Machinery fault diagnostic method based on numerical simulation driving partial transfer learning. Sci China Tech Sci, 2023, 66: 3462–3474, https://doi.org/10.1007/s11431-023-2496-6

1 Introduction

A wide range of applications for rotating machinery in the manufacturing industry is available. The critical components of mechanical systems, such as bearings and gears, inevitably develop various faults because of their long-term operation in a harsh working environment, which can affect the performance of running equipment and, in severe cases, result in complete machinery failure [1–5]. Therefore, identifying mechanical faults is critical to ensure that the equipment continues to operate normally.

Mechanical intelligent fault diagnosis is gaining momentum, and deep learning (DL)-based data-driven approaches are ushering in a broad prospect for engineering applications because of the strong feature learning ability of DL [6–8]. Several artificial intelligence (AI) models [9–12] have recently sprung up, contributing significantly to modern intelligent fault diagnosis processes. According to ref. [13], a novel stacked autoencoder (SAE) model with lossless and nonnegative constraints was proposed to supplement the traditional SAE, which has higher robustness. In ref. [14], a transferable convolutional neural network (CNN) was developed, which was pretrained using source domain samples and fine-tuned according to specific diagnostic tasks. Xiang et al. [15] developed a novel scheme for detecting faults in a

*Corresponding author (email: jwxiang@wzu.edu.cn)

wind turbine, in which a CNN was cascaded to long short-term memory using an attention mechanism.

However, in engineering scenarios, available data on real-world mechanical systems are scarce, which cannot meet the requirements of AI models for several complete labeled training samples. Moreover, although a few scholars have researched and proposed unsupervised clustering methods for unlabeled data, these methods can only gather the same features and cannot obtain category information. Recently, the finite element method (FEM) has been gaining increasing attention in modern fault diagnosis because of the low cost of obtaining simulation results for reference values. For instance, Mousavi et al. [16] combined the FEM and real intact states to construct training data and used DL for damage detection. Seventekidis and Giagopoulos [17] simulated a structure using the FEM to generate labeled damaged data as training samples for a hierarchical CNN. Padil et al. [18] presented a non-probabilistic method to detect vibration damage and verified it on the numerical and laboratory model.

In particular, an FEM simulation-based personalized diagnosis method (PFEM) was developed, introducing a new approach to address the issue of training sample shortage [19–21]. The FEM was applied to construct finite element simulation analysis models of mechanical systems in the method, and several fault samples of the corresponding mechanical system could be obtained by simulation, which can be adopted as training samples for AI models to compensate for the difficulty in obtaining fault samples in a few key parts. Numerical simulation provides the possibility of obtaining various fault samples under any working conditions. However, there are still limitations to this approach, such as unavoidable discrepancies owing to differences between the simulation environment, boundary conditions, etc., and the actual working environment, which degrades classification precision [21].

Recently, generative adversarial networks (GANs) [22] have gained increasing attention because they play a significant role in learning the potential features of a dataset and expanding it. Owing to the generation ability of GANs, many researchers have used them to solve the insufficient data problem [23,24], and some scholars have extended GANs to mechanical fault diagnosis to improve classification accuracy. Shao et al. [25] developed a new type of GAN model, in which label information was considered to assist in producing realistic synthesized signals that can be used as augmented data. Luo et al. [26] achieved imbalanced fault diagnosis by adding conditions to GANs, especially the discriminator was separated from the trained model as a classifier for fault classification. In particular, Gao et al. [27,28] presented an FEM simulation-based GAN method (GFEM), which was performed on the basis of PFEM, and used GANs to enlarge samples to obtain improved classification accuracy. However, the generalization ability of GFEM remains a problem to be solved.

Nevertheless, transfer learning provides hope for enhancing the generalization ability of models [29]. It can learn domain-invariant features, which means that the model can achieve good performance, although it is used in domains with different data distributions [30]. However, the categories of the collected real-world test samples are not necessarily the same as those of the training samples. Therefore, partial transfer learning, as an important branch, is more suitable for most engineering scenarios, which refers to the fact that the types of faults in the target domain (training samples) are only a fraction of those in the source domain (test samples) [31]. For instance, an importance-weighted adversarial network (IWAN) was presented in ref. [32], where an additional discriminator was used to identify source domain samples outside the common fault class. Li et al. [33] introduced weighted learning techniques into a partial transfer learning network to exclude unrelated source domain samples and aligned the distribution of samples with the same categories in two domains. Li and Zhang [34] presented multiple classification modules to fight against the discriminator to obtain prediction consistency and used maximum mean discrepancy to reduce distribution discrepancy. Deng et al. [35] designed a novel deep transfer learning model called double-layer attention-based GAN to solve the partial transfer learning problem across different machines. Liu et al. [36] developed a weighted domain discriminator to weight the sample space of the source domain and aligned it with the target domain. Li et al. [37] proposed a class-weighted adversarial network for partial domain adaptation. By assigning class-level weights to the source categories, the relationship between the source and target domains can be intuitively presented. In summary, partial transfer learning can address the weak generalization ability of models caused by cross-domain asymmetry.

Motivated by the abovementioned studies, a numerical simulation-based partial transfer learning method for machinery fault diagnosis is presented to solve the problems of poor diagnostic precision and weak generalization ability of GFEM. The key viewpoints of this study are as follows: (1) Complete simulation samples of different types of faults are acquired by numerical simulations and further augmented by GANs to construct adequate training samples. (2) The application of the partial transfer learning network can avoid the problem of negative transfer, resulting from the class imbalance between training and test samples while minimizing domain shift. (3) The presented idea is an extension of GFEM, which not only achieves higher fault identification accuracy but also has stronger generalization ability. Consequently, unknown samples collected from critical components such as bearings and gears of real-world operating mechanical systems can be accurately classified.

The remainder of this article is constituted as follows. Theoretical background, including PFEM, GFEM, and the specific partial transfer learning network structure used in this article, is detailed in Section 2. In Section 3, the structure of this idea is presented. In Section 4, experimental investigations are performed. Conclusions are drawn in Section 5.

2 Theoretical background

2.1 Personalized diagnosis method

In actual engineering applications, using physical sensors directly in some key parts is difficult, thereby resulting in missing fault samples. Thus, PFEM [20,21] was proposed to simulate missing fault samples and then complete the types of fault samples. Responding to the precise diagnosis requirements caused by individual differences in mechanical equipment under real-world conditions, numerical simulation methods are adopted to develop agreeable FEM models of mechanical systems to obtain different types of simulation signals reflecting actual operating conditions. The brief steps of PFEM can be summarized as follows.

Step 1: Develop an effective FEM model of the critical components of the mechanical system.

First, an initial FEM model of a mechanical system is established using ANSYS software [38]. Then, update the FEM model with the FEM model updating technology [39]. In general, the critical model properties are repeatedly modified until the cosine similarity between the normal simulation signals and the normal measured signals meets certain requirements. The threshold is generally set to 0.6 [20,21] in engineering applications. Finally, a normal FEM model of the critical components of the mechanical system is established.

Step 2: Perform numerical simulation to acquire the simulation signals.

Predefine the possible fault modes of the mechanical system and then add faults to the normal FEM model. Numerical simulation is performed on the faulty FEM models to obtain FEM simulation signals comprising multiple types of faults. Furthermore, the simulation fault samples can be constructed as training samples for the AI models by preprocessing.

Step 3: Classify faults using AI models.

Similarly, using preprocessed measured signals, the measured fault samples can be constructed as test samples for AI models. The training samples are input into AI models, and eventually, the fault modes of the test samples are detected.

2.2 FEM simulation-based GAN method (GFEM)

The feasibility of PFEM has already been confirmed; however, the diagnosistic accuracy needs to be improved. Therefore, GFEM [27,28], which combines PFEM and GANs, was developed to enlarge samples to obtain improved classification accuracy.

The GAN composition is shown in Figure 1, comprising a generator (G) and discriminator (D). G generates random noise z into signals with the same characteristics by learning the potential statistical characteristics of real signal x. D distinguishes the generated signal $G(z)$ from x as much as possible and determines whether $G(z)$ is fake or real. The overall objective function is represented as follows:

$$L_D = \max_D E_{x\sim p_{\text{data}}(x)}[\log D(x)] + E_{z\sim p_z(z)}[\log(1-D(G(z)))], \quad (1)$$

$$L_G = \min_G E_{z\sim p_z(z)}[\log(1-D(G(z)))]. \quad (2)$$

The training of the two components is alternately performed. The real signals and the signals generated by G are first passed to D, which then predicts which signals are real and fake. Next, the predicted results are checked against the true results, and the binary cross-entropy loss is calculated. The gradient is backpropagated only through D in this step, and its parameters are accordingly optimized. While updating G, the ground truth labels are all labeled as "real" because G is expected to generate signals as similar as possible to real ones. Therefore, when G attempts to fool D, the gradient is backpropagated only through G. The adversarial training continues until it achieves its Nash equilibrium [40]. The trained GAN can be used to generate many samples that have statistical characteristics similar to those of the original ones.

Different from PFEM, the use of a GAN in GFEM can expand the simulation and measured samples. Moreover, the discrepancy between the simulation and measured samples could be suppressed by GAN at a certain level. Thereafter, complete labeled training fault samples could be constructed by combining all measured, simulation, and synthetic fault samples. Eventually, the complete labeled training fault samples are applied to the AI model, and unknown fault samples are used for testing to achieve fault diagnosis. These findings demonstrate that this approach can improve diagnostic precision to some extent compared with PFEM.

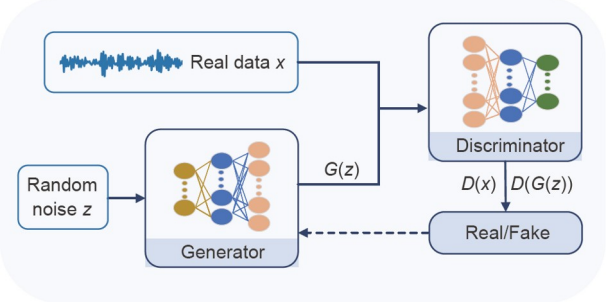

Figure 1 (Color online) GAN overview.

2.3 Partial transfer learning network

2.3.1 *Transfer learning problem definition*

First, some definitions and symbolic representations of transfer learning are introduced in detail. Let $\{x^s, y^s\}=\{(x_i^s, y_i^s)\}_{i=1}^{n_s}$ represent data with labeled information from the source domain D_s and $\{x^t\}=\{x_i^t\}_{i=1}^{n_t}$ data without labeled information from the target domain D_t. n_s and n_t denote the sample sizes in D_s and D_t, respectively, and C_s and C_t denote the corresponding label sets, respectively. $p_s(x)$ and $p_t(x)$ are different marginal distributions, from which x^s and x^t are drawn, respectively. In particular, this study is based on the assumption that D_t and D_s only share part of the label space, specifically $C_t \in C_s$. Partial transfer learning is better suited to real-world diagnostic applications, where x^t belongs to a limited number of categories.

2.3.2 *Importance-weighted adversarial network (IWAN)*

The architecture of the IWAN is illustrated in Figure 2, comprising two feature extractors, two domain discriminators, and a health condition classifier. The feature extractors are denoted by F_s and F_t, which are utilized to extract the features of the two domain samples, respectively. The two domain discriminators are denoted as D_0 and D_1, and the health condition classifier is represented by C.

In the IWAN, F_s and C are first optimized to extract features and accurately classify the source domain samples. The loss function is expressed as follows:

$$\min_{F_s,C} L_s(F_s, C) = -E_{x,y\sim p_s(x,y)} \sum_{k=1}^{K} I_{[k=y]} \log C(F_s(x)), \tag{3}$$

where K represents the fault categories, and $I[\cdot]$ represents an indicator function. Note that the parameters of F_s, which are trained in the previous step, are fixed during the formal adversarial training procedure. Next, we maximized the domain classification error of D_0, expressed as follows:

$$\min_{D_0} L D_0(D_0, F_s, F_t) = -E_{x\sim p_s(x)}\left[\log D_0(F_s(x))\right] + E_{x\sim p_t(x)}\left[\log\left(1 - D_0(F_t(x))\right)\right]. \tag{4}$$

Assuming that D_0 has achieved convergence to the optimal value based on the current F_t, the output of D_0 can be expressed as the probability that a sample originates from a certain domain. Therefore, the activations of D_0 can be adopted to exclude the samples of the source domain that are more important to the target domain. Let D^* represent the optimum value of D_0, and $t=F(x)$ be the extracted feature obtained after processing by the feature extractor. If $D^*(t)\approx 1$, the categories of these samples are unlikely to exist in the shared label space. In this case, the contribution of these samples should be minimized so that D_0 and F_t can ignore them to avoid negative transfer. Conversely, if $D^*(t)$ is smaller, it implies that these samples are most probably from common classes between domains, which should be assigned greater importance weights. In summary, the importance-weighting function is expected to be inversely proportional to $D^*(t)$ and can be described as follows:

$$\tilde{w}(t) = 1 - D^*(t) = \frac{1}{\frac{p_s(t)}{p_t(t)} + 1}. \tag{5}$$

From eq. (5), a small $D^*(t)$ value implies that the category of the sample likely belongs to the common part and then $\tilde{w}(t)$ increases. Note that the density ratio between the source and target characteristics also influences the weighting function, further validating its effectiveness, as the source domain samples outside the boundary are assigned low weights.

To acquire the relative importance according to F_s and current F_t, the weights are normalized to obtain $w(t)$. The resulting weights are then assigned to the source domain features such that the common category of source domain features can be given larger weights, whereas unrelated features are given smaller weights. The weighting function is defined as a function of D_0; therefore, the results generated

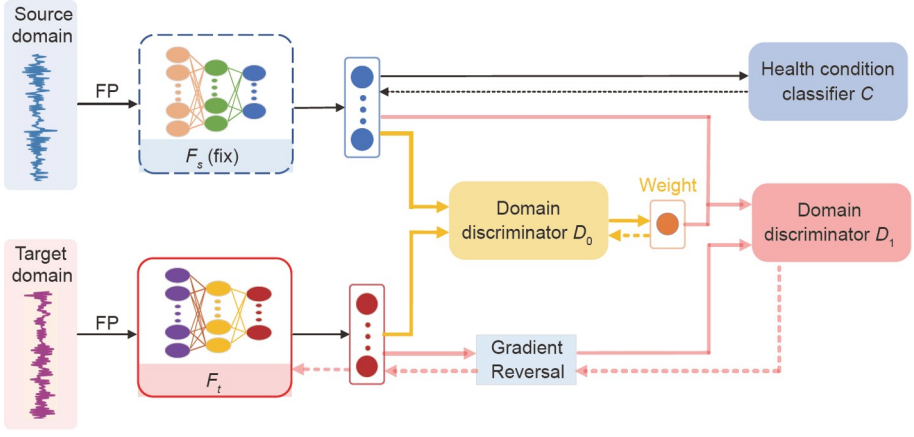

Figure 2 (Color online) Composition of the IWAN.

by the adversarial game between F_t and D_0 cannot reduce the Jensen-Shannon divergence between the two densities if the weights are applied to the same domain discriminator. Based on this situation, this problem is solved by applying a second domain discriminator D_1 to compare the two domain features. Confusing the different domain features by maximizing the loss of D_1 allows F_t to learn domain-invariant features.

Moreover, the entropy minimization principle [41] is used to restrain F_t. Consequently, the third optimization object can be described as follows:

$$\begin{aligned}\min_{F_t}\max_{D_1} L_w(C,D_1,F_s,F_t) = \gamma E_{x\sim p_t(x)} H\big(C(F_t(x))\big)\\ +\lambda\big(E_{x\sim p_s(x)}\big[w(t)\log D_1(F_s(x))\big]\\ +E_{x\sim p_t(x)}\big[\log\big(1-D_1(F_t(x))\big)\big]\big),\end{aligned} \tag{6}$$

where γ and λ denote tradeoff parameters and $H(\cdot)$ represents the information entropy function. F_s and C are optimized in advance using the source domain samples and are not updated in the subsequent training process. In the formal training phase, D_0, D_1, and F_t are simultaneously optimized. D_0 is only used to obtain the relevance weights of the source domain samples based on F_s and current F_t, whereas D_1 plays an adversarial game with F_t to update F_t. Notably, the adversarial game between F_t and D_1 is resolved using the gradient reversal layer (GRL) [42].

3 The presented method structure

Inspired by previous research [20,21,27,28], a numerical simulation-based partial transfer learning method for mechanical fault diagnosis is proposed to classify unknown samples collected from real-world engineering applications. Figure 3 shows the specific procedure of the proposed method, which comprises the following three stages.

Stage 1: Create the FEM model to acquire FEM simulation fault samples.

At this point, FEM is used to construct a consensual simulation model of critical components in a mechanical system, and numerical simulation is performed to acquire FEM simulation samples comprising different types of faults. The problem of the shortage of complete labeled training fault samples can be solved.

Stage 2: Obtain complete source domain training samples.

Taking the original FEM simulation samples as a template, a GAN is used to generate a significant number of synthetic simulation samples to enlarge the sample size and reduce the discrepancy between the two types of samples to some extent. Thereafter, all synthetic simulation and FEM simulation fault samples are finally added together to construct complete source domain training samples. In addition, the dataset has been expanded, which is beneficial for training the model.

Stage 3: Train IWAN to identify faults in the mechanical system.

In practice, collected real-world test samples may not share the same label space as training samples. Therefore, IWAN is adopted for partial transfer learning based on the above-mentioned situation to prevent negative transfer. Specifically, IWAN is applied to the constructed complete source domain samples and is further used to identify unknown target domain samples collected from real-world mechanical systems in operation.

4 Experimental investigations

In this section, experimental investigations are performed based on bearing and gearbox datasets to verify the effectiveness of the proposed method. All data processing is performed on a PC with an NVIDIA GPU GeForce GTX 1050Ti, CPU Core i7-9700 3 GHz, 32 GB RAM, Tensorflow 2.3, MATLAB 2018, and Cuda 10.1.

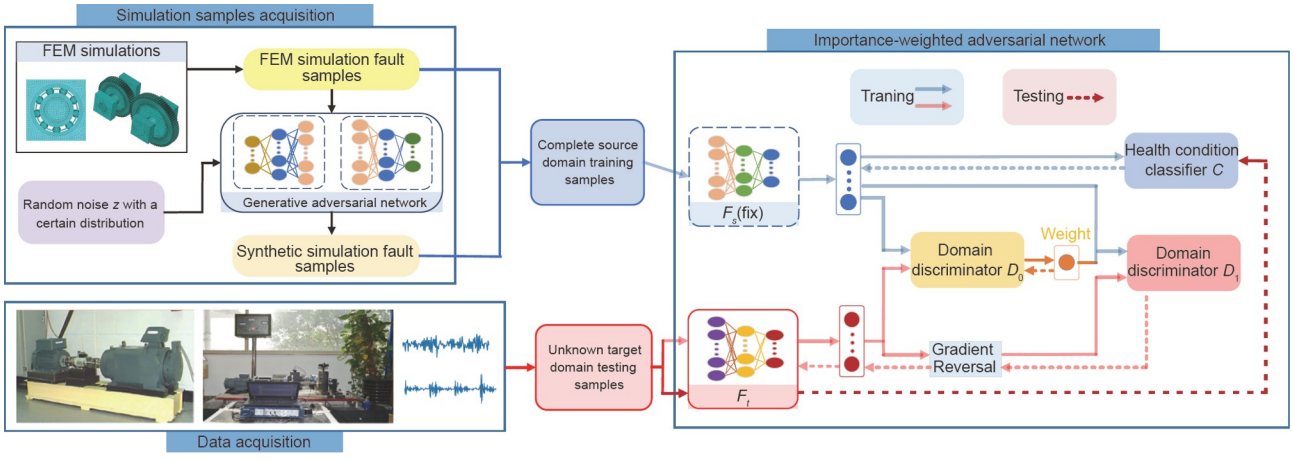

Figure 3 (Color online) Procedure of the presented method.

4.1 Experiment setup

4.1.1 Gearbox dataset

To evaluate the practicability of the proposed method, a gear fault dataset collected from our laboratory's gearbox experimental test bench is used for analysis, as depicted in Figure 4, where the various components of the test bench have been labeled. In particular, an ECON AVANT MI-7016 16-channel vibration signal acquisition instrument is used to acquire vibration signals, and the model of the acceleration sensor is AI002 with a sensitivity of 2.005 mV/ms^{-2}. A driving gear with 55 teeth, a driven gear with 75 teeth, and 4 cylindrical roller bearings and shafts constitute the gear transmission system. The driving shaft rotates at 1474 r/min, and signals from an accelerator sensor mounted at the drive end of the driving shaft are collected at 5120 Hz sampling frequency.

The gear faults are shown in Figure 5(a)–(d), which include driving gear tooth crack (TCF), driven gear tooth break (TBF), driving gear tooth break (GBF), and driving gear tooth spalling (TSF), respectively. For experimental investigations, six gear health conditions are considered: TCF, TSF, GBF, compound fault of TSF and TBF (TSBF), compound fault of GBF and TBF (GTBF), and normal (N).

4.1.2 Bearing dataset

The public bearing dataset from Case Western Reserve University (CWRU) [43] is used to further validate the generalizability of the developed idea. Signals acquired at a sampling frequency of 12000 Hz from accelerometers mounted at the drive-end bearing rotated at a load of 0 are used in the experimental investigations. Six fault types are considered: inner race fault (named IF07 and IF21), ball fault (named BF07 and BF21), and outer race fault (named OF07 and OF21), where 07 and 21 indicate that the fault severity degrees are 0.007 and 0.021 inches, respectively.

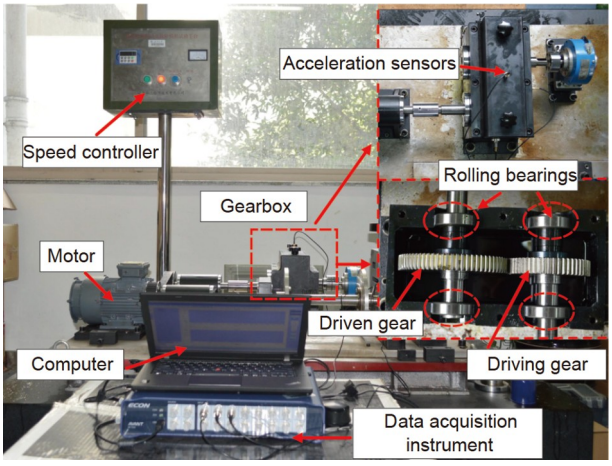

Figure 4 (Color online) Gearbox experimental test rig.

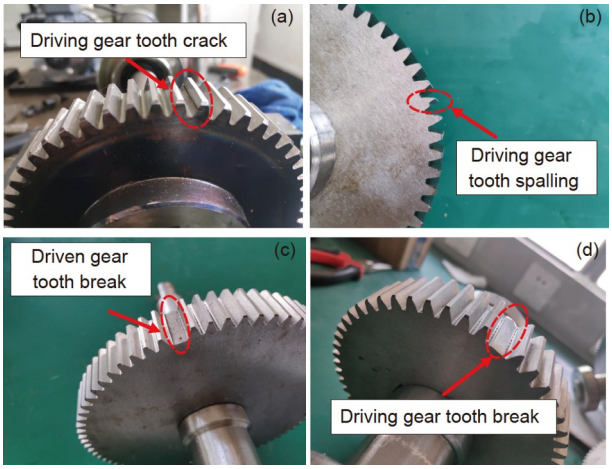

Figure 5 (Color online) Types of gear faults. (a) TCF; (b) TSF; (c) TBF; (d) GBF.

4.2 Design of fault diagnosis experiments

To address the issue of class mismatch in the training and test samples for practical applications, four groups of experiments are designed on the gear and bearing datasets, presented in Tables 1 and 2 below. Taking the task T2 for instance, the target domain fault samples belong to four types: TSF, GBF, TSBF, and GTBF. The source domain samples comprise synthetic and FEM simulation fault samples.

4.3 FEM model construction

4.3.1 Construct the FEM model of the gearbox

Complete simulation fault samples comprising different types of faults can be obtained from the FEM models of faulty gears. Specifically, the FEM model of the gearbox is developed using the ANSYS software. To improve the efficiency of the simulation calculation, the transmission enclosure is reasonably simplified to several bearing seats and

Table 1 Fault diagnosis experiments on the gearbox dataset

Tasks	Source domain	Target domain
T1	N, TCF, TSF, GBF, TSBF, GTBF	TCF, TSF, GBF, TSBF, GTBF
T2		TSF, GBF, TSBF, GTBF
T3		TCF, GBF, GTBF
T4		TSF, TSBF

Table 2 Fault diagnosis experiments on CWRU bearing dataset

Tasks	Source domain	Target domain
T5	IF07, OF07, BF07, IF21, OF21, BF21	IF07, OF07, BF07, IF21, OF21
T6		IF07, OF07, BF07, OF21
T7		IF07, OF07, OF21
T8		BF07, OF21

the properties of the stiffness and damping are simulated using contact pairs.

More specifically, the element of SOLID164 is applied to create the meshing of the gear body, and SHELL163 is employed to produce the meshing of the surface driving shaft to apply the rotating loading. In the simulation modeling, referring to the actual material parameters, all components are defined as linear elastic materials, the specific parameters of which can be found in Table 3. In addition, several contact pairs are created in the gearbox model, comprising four pairs on the shaft and bearing seats and one pair between the two gears. All degrees of freedom (DOF) on the outer surface of the four bearing seats are limited in accordance with the actual working conditions.

The model updating technology in ref. [44] is used in the procedure of optimizing the normal FEM model to make the FEM model correspond more closely to the experimental gearbox. According to the modulation mechanism of the vibration response of the gearbox, signals are processed by bandpass filtering to effectively extract model parameter information such as gear meshing stiffness and damping. Specific bandpass filtering processing details can be found in ref. [21]. In addition, the reliability of the FEM model is verified by contrasting the similarity of the simulation and actual signals using cosine similarity in the time domain [45]. According to the main boundary conditions determined in ref. [21], the FEM model is created. The updated parameters are listed in Table 3, and the FEM meshing of the normal gears is depicted in Figure 6(a). The final calculated cosine similarity value is 0.742, which indicates that the developed FEM model is reliable.

Subsequently, by adding several faults, as shown in Figure 6(b)–(f), to the developed FEM model, different types of FEM simulation vibration signals can be generated through numerical simulation. TSF, GBF, and GTBF faults are randomly selected as examples, and the time-domain spectrograms of the simulation and corresponding actual signals are depicted in Figure 7. The two signals are well matched, which again demonstrates the reliability of the FEM model.

Table 3 Gearbox FEM model parameter list

Parameters	Value
Material density	7860 kg/m³
Elastic modulus	2.06×10^{11} Pa
Poisson's ratio	0.3
Friction coefficient	0.08
Bearing synthetic damping ratio	0.09
Bearing comprehensive contact stiffness	0.16
Gear contact damping ratio	0.005
Gear meshing stiffness	0.15

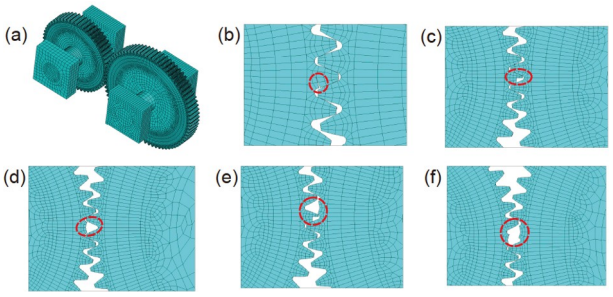

Figure 6 (Color online) Gearbox FEM model and fault types. (a) Gearbox model; (b) TCF; (c) TSF; (d) GBF; (e) TSBF; (f) GTBF.

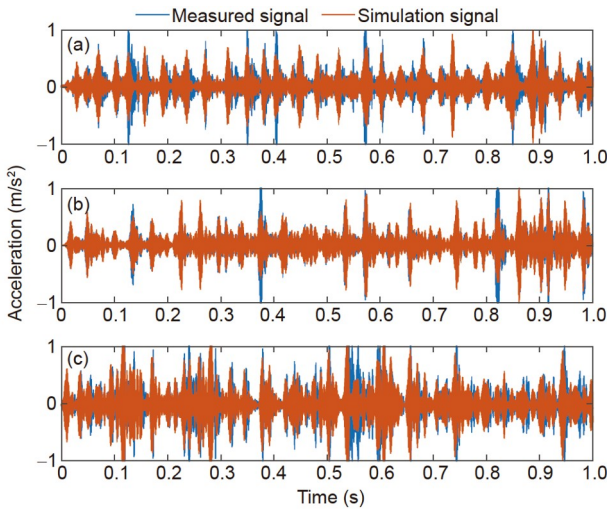

Figure 7 (Color online) Time-domain spectrograms of simulation and corresponding actual signals of gears. (a) TSF; (b) GBF; (c) GTBF.

4.3.2 *Construct the bearing FEM model*

A three-dimensional FEM model is also created by the ANSYS software based on the geometric dimensional parameters of the SKF6250 bearing from the CWRU. Note that the bearing seat and shaft are also included in the modeling, considering the actual working conditions. The FEM model is shown in Figure 8(a).

Similar to the modeling of gears, SOLID164 and SHELL163 are also used to create a simulation model. All elements are defined as linear elastic materials, and the material parameter setting is the same as that for the gear transmission system. The inner ring and shaft synchronously rotate, and the bearing seat is fixedly connected to the bearing outer ring and has restricted DOF at all nodes on the outer surface. Contact pairs are constructed between the rollers and inner and outer rings. The static friction coefficient is set to 0.32, and the dynamic friction coefficient is set to 0.16, according to ref. [27]. In the procedure of updating the normal simulation model, the model updating technology previously described is also used to determine the main boundary conditions. Repeatedly update the parameters such as gravity, eccentric load, and inner preload and obtain the corresponding simulation signals, and then calculate the

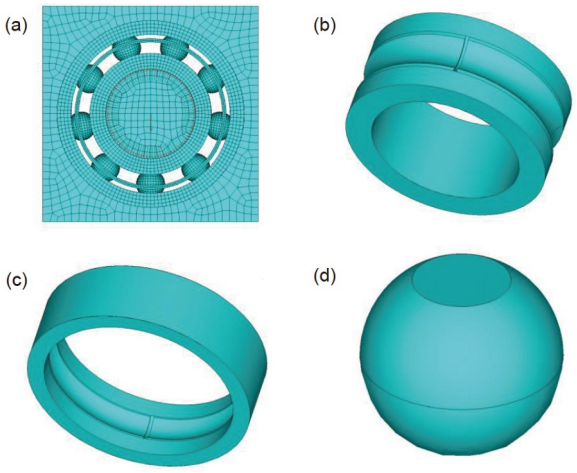

Figure 8 (Color online) Bearing FEM model and fault types. (a) Bearing model; (b) IF; (c) OF; (d) BF.

cosine similarity until the result satisfies the condition. The essential properties of the updated bearing FEM model are provided in Table 4, according to ref. [20]. The associated cosine similarity value is 0.618, exceeding the threshold value.

Figure 8(b)–(d) shows the FEM and geometry of faults of different types added to the normal FEM model. Fault FEM simulation vibration samples can be obtained by performing a numerical calculation from the model with the relative fault. To visually display the simulation and measured signals, the time-domain waveforms of IF07, OF07, and BF07 are shown in Figure 9. A slight difference can be found between the two signals but within a reasonable range.

4.4 Obtain complete source domain training samples

The discrepancy between the numerical simulation and measured samples is inescapable. To further reduce the difference and enlarge FEM simulation fault samples, a GAN is used to generate several synthetic simulation samples. In this study, the FEM simulation fault samples are used as real samples in the GAN and the random noise is sampled from a uniform distribution (z~$u(-1,1)$). The specific structure and parameters of G and D are listed in Table 5, where BN denotes the batch normalization layer. Thereafter, complete source domain training samples can be constructed by combining synthetic simulation fault samples and the original FEM simulation samples.

The frequency spectra of the simulation signals for the gears and bearing are shown in Figures 10 and 11, including the simulation signals obtained by the FEM and synthetic simulation signals generated from the original FEM signal. To further judge the degree of matching of frequency characteristics, only the frequency spectrum with a specific range of frequency values is displayed in the figures. The fault frequency characteristic of the synthetic simulation signal

Table 4 Gearbox FEM model parameter list

Contact parameters	Value	Load parameters	Value
Normal contact stiffness factor	0.12	Gravity load of shaft	495 N
Dynamic friction factor	0.16	Eccentric load	0.1 MPa
Static friction factor	0.32	Inner rotating speed	1797 r/min
Viscous damping factor	0.02	Inner preload	1 MPa

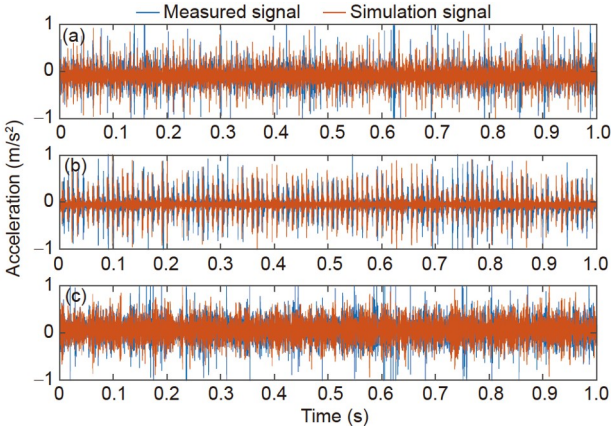

Figure 9 (Color online) Time-domain spectrograms of simulation and corresponding actual signals of bearing. (a) IF07; (b) OF07; (c) BF07.

Table 5 Specific structures of the GAN

Module	Layer	Number of channels/ size/stride/activation
G	Dense	150*64/1/*/*
	BN	/
	Activation	LeakyReLu
	Reshape	/
	Deconvolution	16/(3,1)/2/*
	BN	/
	Activation	LeakyReLu
	Deconvolution	8/(3,1)/2/*
	BN	/
	Activation	LeakyReLu
	Deconvolution	1/(3,1)/2/Tanh
	BN	/
	Activation	LeakyReLu
D	Reshape	/
	Convolution	8/(3,1)/2/*
	Activation	LeakyReLu
	Convolution	16/(3,1)/2/*
	Activation	LeakyReLu
	Flatten	/
	Dense	1/1/*/Sigmoid

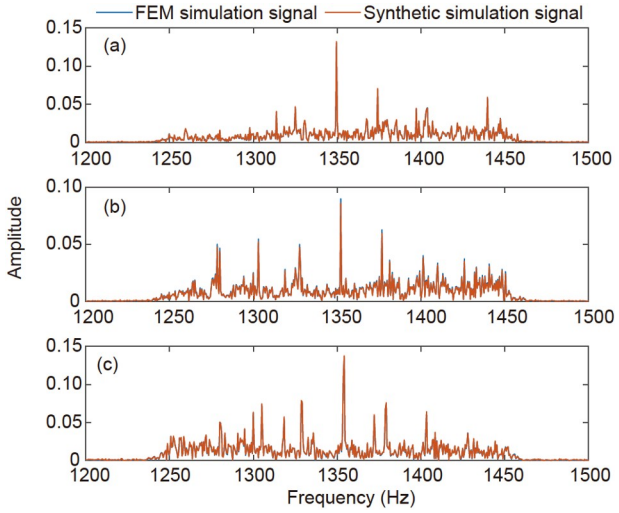

Figure 10 (Color online) Frequency spectra of simulation signals for gears. (a) TSF; (b) GBF; (c) GTBF.

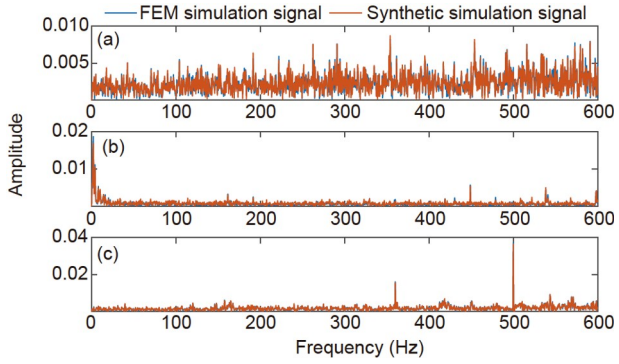

Figure 11 (Color online) Frequency spectra of simulation signals for bearing. (a) IF07; (b) OF07; (c) BF07.

matches to that of the FEM simulation signal.

4.5 Fault diagnosis based on IWAN

In this section, the detection of designated fault diagnostic tasks is performed. In the case of the gearbox dataset, the complete source domain training samples are formed by 1200 (200×6) fault samples, with 250 data points in each sample. Correspondingly, the unlabeled measured samples are considered as the target domain, and 80 fault samples with 250 data points are available for each class. For the CWRU bearing dataset, the source domain comprises 1800 (300×6) fault samples with the length of each sample equal to 400 and the target domain sample size for each category is 300 of the equivalent length. Considering task T6, for instance, 1200 (300×4) fault samples in the target domain are observed.

The details of the IWAN parameters are set, as described below. F_t is achieved using several convolutional, pooling, and fully connected layers, and C, D_0, and D_1 are composed of fully connected layers. Their specific constructions are listed in Table 6, where GAP represents the global average pooling layer and GRL is the gradient reversal layer. The Adam optimization algorithm [46] is used to update the IWAN model, where the learning rates of F_t, C, D_0, and D_1 are defined as 1×10^{-3}, 5×10^{-4}, 5×10^{-4}, and 5×10^{-4}, respectively. The parameters γ and λ are defined as 1 for simplicity [34]. The batch size is set as 32. Note that half of each batch comprises the complete source domain fault samples, and the second half comprises the target domain fault samples.

4.6 Experimental results and discussion

In this study, PFEM [21], FEM simulation-based GAN method (GFEM) [27], and unsupervised clustering method (UCM) [47] are implemented for comparison. Specifically, in PFEM, the source domain training samples comprise only 240 (40×6) and 180 (30×6) FEM simulation fault samples for the gear and bearing datasets, respectively. In addition, a CNN is adopted as the classifier for PFEM and GFEM. In the UCM, DCGAN is used to extract features [47] from unlabeled measured samples in the target domain and then perform clustering using the k-means clustering algorithm.

4.6.1 Experimental results analysis of gearbox dataset

The experimental results obtained from the four gearbox diagnosis tasks are presented in Table 7. Note that the effectiveness of the UCM can be analyzed using the following indicators: adjusted rand index (ARI), normalized mutual information (NMI), and purity. The test accuracy obtained on D_t is used to evaluate the performance of other methods. Comparing these results, the proposed method has the best

Table 6 Specific structures of IWAN

Module	Layer	Number of channels/size/stride/activation
F_t	Convolution	8/(5,1)/2/ReLu
	Max Pooling	/
	Convolution	16/(5,1)/2/ReLu
	Convolution	32/(5,1)/2/ReLu
	Convolution	64/(5,1)/2/ReLu
	Convolution	128/(5,1)/2/ReLu
	Convolution	256/(5,1)/2/ReLu
	GAP	/
	Dense	32/1/*/*
C	Dense	32/1/*/ReLu
	Dense	6/1/*/Softmax
D_0	Dense	32/1/*/ReLu
	Dense	1/1/*/Sigmoid
D_1	GRL	/
	Dense	32/1/*/ReLu
	Dense	1/1/*/Sigmoid

Table 7 Experimental results for gearbox diagnosis tasks

Task	PFEM (%)	GFEM (%)	UCM			Proposed (%)
	D_t	D_t	ARI	NMI	Purity	D_t
T1	90.49	93.00	0.947	0.951	0.973	100
T2	91.87	96.88	0.979	0.970	0.988	99.38
T3	92.50	94.16	0.982	0.974	0.996	99.17
T4	91.84	94.99	0.985	0.977	0.998	100
Avg	91.68	94.76	0.973	0.968	0.989	99.64

classification performance in the different tasks, with an average diagnostic accuracy of 99.64%. More specifically, the average accuracy of PFEM and GFEM is lower than that of the proposed method by 7.96% and 4.64%, respectively. However, the average classification accuracy of GFEM is higher than that of PFEM, proving that the adoption of a GAN can compensate for the discrepancy between the FEM simulation and measured fault samples. Furthermore, the use of IWAN in the proposed method solves the generalization ability of GFEM and can obtain more satisfactory classification results. For the UCM, the value of each evaluation metric is close to 1, indicating that the unsupervised results are satisfactory. However, labeled information cannot be obtained from the UCM; thus, using the FEM to obtain labeled training samples is necessary.

To show the generalization capacity of the proposed idea, t-SNE [48] is employed for feature visualization. Considering fault diagnosis experiment T2 as an illustration, the features obtained using PFEM, GFEM, and the proposed method are visualized in Figure 12. From Figure 12(a) and (b), the features of different domains generated using PFEM and GFEM are not well separated. As shown in Figure 12(c), the proposed method can aggregate the characteristics of the same class from different domains, and some distance between samples with different types of categories is observed, which is beneficial to the classification outcome. In summary, these results certify that the proposed method has satisfactory classification accuracy and generalization ability.

4.6.2 *Experimental results analysis of bearing dataset*

The classification results for the four experiments of the bearing dataset are presented in Table 8. The test accuracy of the proposed method in the four diagnostic tasks is 99.33%, 99.17%, 100%, and 99.67%, respectively. Compared with the other methods, the mean diagnosis precision of the proposed method is 99.54%, which is higher than that of PFEM and GFEM, which are 91.89% and 96.41% respectively. The average accuracy of PFEM is over 90%, which confirms that the simulation signals obtained by numerical simulations can replace the measured signals collected from real-world operating mechanical systems to some degree. Moreover, the improvement effect of the IWAN on the generalization ability is again reflected by comparing it with GFEM. Similar to the gearbox dataset, the clustering effect of the UCM on the bearing dataset is also excellent; however, the problem

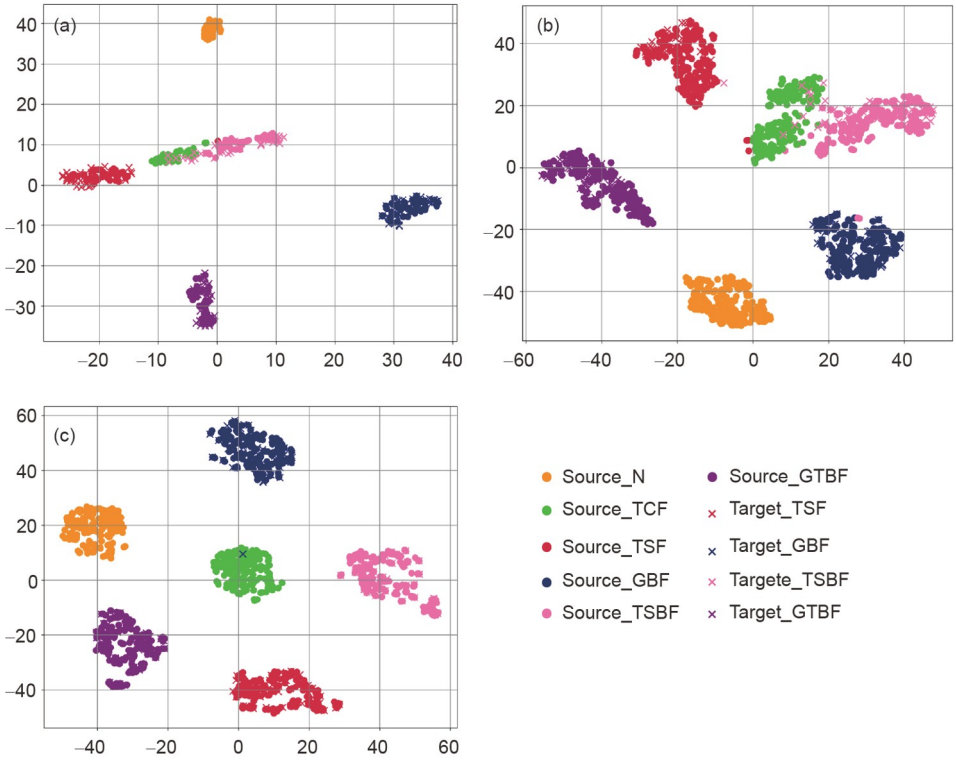

Figure 12 (Color online) Feature visualization for gears. (a) PFEM; (b) GFEM; (c) proposed.

Table 8 Experimental results for bearing diagnosis tasks

Task	PFEM (%)	GFEM (%)	UCM			Proposed (%)
	D_t	D_t	ARI	NMI	Purity	D_t
T5	92.71	96.77	0.985	0.973	0.986	99.33
T6	91.53	97.55	0.984	0.969	0.993	99.17
T7	91.33	95.33	1.0	1.0	1.0	100
T8	92.00	95.99	1.0	1.0	1.0	99.67
Avg	91.89	96.41	0.992	0.986	0.995	99.54

of not being able to obtain category information remains unresolved.

The features of the bearing samples are also displayed by t-SNE to explore the effect of the proposed method in reducing distribution differences. The features acquired by PFEM, GFEM, and the proposed method in the fault diagnosis task T6, which is randomly chosen, are visualized in Figure 13. As shown in Figure 13(a), the features of a few types of faults of different domains are not stacked together, which shows that differences in the distribution between the two domains are still present. Figure 13(b) shows that the feature distribution between the two domains is closer than that of PFEM because of the use of a GAN. The proposed method has stronger generalization and classification capabilities than GFEM, as evidenced by the fact that the features of Figure 13(c) are more concentrated than those of Figure 13(b).

5 Conclusion

To improve the classification precision and generalization ability of GFEM, numerical simulation-based partial transfer learning is developed to classify unknown samples collected from critical components such as bearings and gears of real-world operating mechanical systems. Unlike GFEM, the adoption of partial transfer learning will learn common features from simulation samples and further classify unknown measured samples. Experimental investigations on bearings and gears with faults demonstrate that the proposed method can identify faults accurately and has a strong generalization ability. Compared with PFEM, GFEM, and the UCM, the essential contributions of this article can be summarized in the following sections: (1) Considering the scarcity of labeled training samples available in engineering practice, this study uses numerical simulation to obtain simulation signals of various fault categories. Sufficient numbers of samples are further expanded using a GAN. (2) Through the adversarial training process and weighting operation of the IWAN, the proposed method learns the common characteristics of the simulation and measured samples and reduces the data distribution difference, improving classification accuracy. This method holds the promise of promoting the successful application of FEM and DL models to intelligent fault diagnosis in real-world mechanical systems in operation. To better align with the data situation in engineering practice, an open set domain adaptation study,

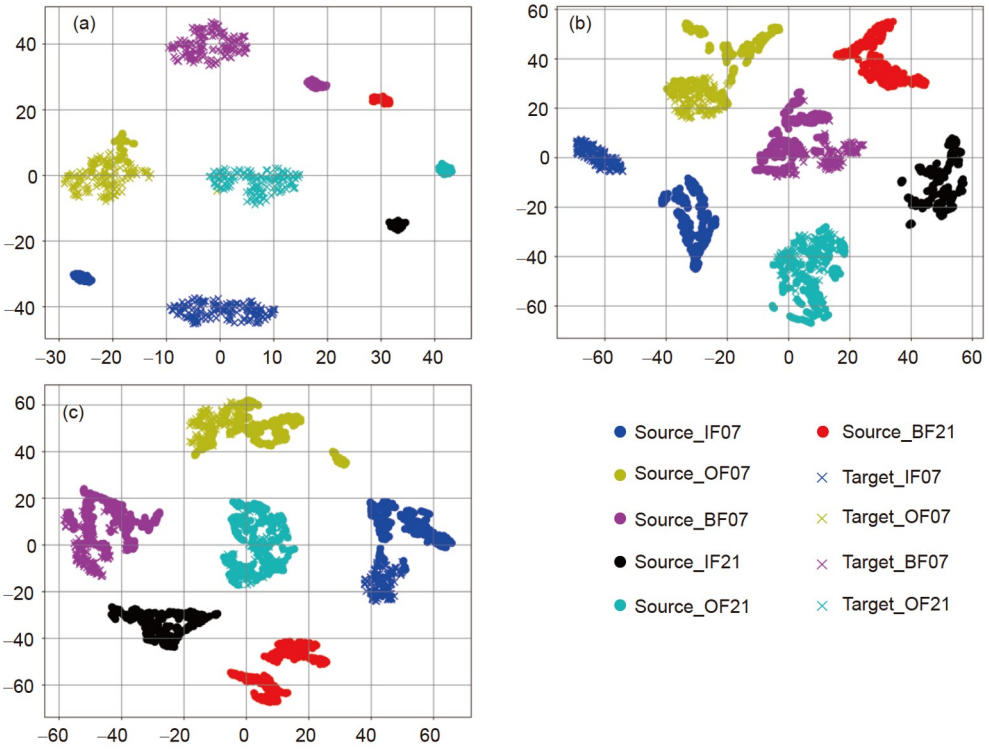

Figure 13 (Color online) Feature visualization for bearing. (a) PFEM; (b) GFEM; (c) proposed.

where some additional faults occur on testing machines that do not belong to the source domain classes, will be explored in the future.

This work was supported by the National Natural Science Foundation of China (Grant No. U1909217), the Zhejiang Natural Science Foundation of China (Grant No. LD21E050001), and the Wenzhou Major Science and Technology Innovation Project of China (Grant No. ZG2020051).

1 Jin Y R, Qin C J, Zhang Z N, et al. A multi-scale convolutional neural network for bearing compound fault diagnosis under various noise conditions. Sci China Tech Sci, 2022, 65: 2551–2563
2 Zhou X, Zhou H C, He Y M, et al. Harmonic reducer *in-situ* fault diagnosis for industrial robots based on deep learning. Sci China Tech Sci, 2022, 65: 2116–2126
3 Liu Y Q, Chen Z G, Wang K Y, et al. Surface wear evolution of traction motor bearings in vibration environment of a locomotive during operation. Sci China Tech Sci, 2022, 65: 920–931
4 Di Z Y, Shao H D, Xiang J W. Ensemble deep transfer learning driven by multisensor signals for the fault diagnosis of bevel-gear cross-operation conditions. Sci China Tech Sci, 2021, 64: 481–492
5 Huang H R, Li K, Su W S, et al. An improved empirical wavelet transform method for rolling bearing fault diagnosis. Sci China Tech Sci, 2020, 63: 2231–2240
6 Han Z Z, Huang Y Z, Li J, et al. A hybrid deep neural network based prediction of 300 MW coal-fired boiler combustion operation condition. Sci China Tech Sci, 2021, 64: 2300–2311
7 Shao H D, Li W, Cai B P, et al. Dual-threshold attention-guided GAN and limited infrared thermal images for rotating machinery fault diagnosis under speed fluctuation. IEEE Trans Ind Inf, 2023, 19: 9933–9942
8 Chen M Z, Shao H D, Dou H X, et al. Data augmentation and intelligent fault diagnosis of planetary gearbox using ILoFGAN under extremely limited samples. IEEE Trans Rel, 2023, 72: 1029–1037
9 Liu G K, Shen W M, Gao L, et al. Active label-denoising algorithm based on broad learning for annotation of machine health status. Sci China Tech Sci, 2022, 65: 2089–2104
10 Chao Q, Gao H H, Tao J F, et al. Adaptive decision-level fusion strategy for the fault diagnosis of axial piston pumps using multiple channels of vibration signals. Sci China Tech Sci, 2022, 65: 470–480
11 Chen X K, Shao H D, Xiao Y M, et al. Collaborative fault diagnosis of rotating machinery via dual adversarial guided unsupervised multi-domain adaptation network. Mech Syst Signal Process, 2023, 198: 110427
12 Qin C J, Wu R H, Huang G Q, et al. A novel LSTM-autoencoder and enhanced transformer-based detection method for shield machine cutterhead clogging. Sci China Tech Sci, 2023, 66: 512–527
13 Li W X, Shang Z W, Gao M S, et al. A novel deep autoencoder and hyperparametric adaptive learning for imbalance intelligent fault diagnosis of rotating machinery. Eng Appl Artif Intell, 2021, 102: 104279
14 Chen Z Y, Gryllias K, Li W H. Intelligent fault diagnosis for rotary machinery using transferable convolutional neural network. IEEE Trans Ind Inf, 2019, 16: 339–349
15 Xiang L, Wang P H, Yang X, et al. Fault detection of wind turbine based on SCADA data analysis using CNN and LSTM with attention mechanism. Measurement, 2021, 175: 109094
16 Mousavi Z, Varahram S, Ettefagh M M, et al. Deep neural networks-based damage detection using vibration signals of finite element model and real intact state: An evaluation via a lab-scale offshore jacket structure. Struct Health Monit, 2021, 20: 379–405
17 Seventekidis P, Giagopoulos D. A combined finite element and hierarchical deep learning approach for structural health monitoring: Test on a pin-joint composite truss structure. Mech Syst Signal Process, 2021, 157: 107735
18 Padil K H, Bakhary N, Abdulkareem M, et al. Non-probabilistic method to consider uncertainties in frequency response function for vibration-based damage detection using artificial neural network. J Sound Vib, 2020, 467: 115069
19 Xiang J W, Zhong Y T. A novel personalized diagnosis methodology using numerical simulation and an intelligent method to detect faults in a shaft. Appl Sci, 2016, 6: 414
20 Xiang J W. Numerical simulation driving generative adversarial networks in association with the artificial intelligence diagnostic principle to detect mechanical faults (in Chinese). Sci Sin Tech, 2021, 51: 341–355
21 Liu X Y, Huang H Z, Xiang J W. A personalized diagnosis method to detect faults in gears using numerical simulation and extreme learning machine. Knowledge-Based Syst, 2020, 195: 105653
22 Goodfellow I, Pouget-Abadie J, Mirza M, et al. Generative adversarial nets. Adv Neural Inf Process Syst, 2014, 27: 2672–2680
23 Zhu Q X, Hou K R, Chen Z S, et al. Novel virtual sample generation using conditional GAN for developing soft sensor with small data. Eng Appl Artif Intell, 2021, 106: 104497
24 Pei L L, Sun Z Y, Xiao L Y, et al. Virtual generation of pavement crack images based on improved deep convolutional generative adversarial network. Eng Appl Artif Intell, 2021, 104: 104376
25 Shao S Y, Wang P, Yan R Q. Generative adversarial networks for data augmentation in machine fault diagnosis. Comput Industry, 2019, 106: 85–93
26 Luo J, Huang J Y, Li H M. A case study of conditional deep convolutional generative adversarial networks in machine fault diagnosis. J Intell Manuf, 2021, 32: 407–425
27 Gao Y, Liu X Y, Xiang J W. FEM simulation-based generative adversarial networks to detect bearing faults. IEEE Trans Ind Inf, 2020, 16: 4961–4971
28 Gao Y, Liu X Y, Huang H Z, et al. A hybrid of FEM simulations and generative adversarial networks to classify faults in rotor-bearing systems. ISA Trans, 2021, 108: 356–366
29 Long M S, Cao Y, Cao Z J, et al. Transferable representation learning with deep adaptation networks. IEEE Trans Pattern Anal Mach Intell, 2019, 41: 3071–3085
30 Pan S J, Yang Q. A survey on transfer learning. IEEE Trans Knowl Data Eng, 2009, 22: 1345–1359
31 Cao Z J, Long M S, Wang J M, et al. Partial transfer learning with selective adversarial networks. In: Proceedings of the IEEE Conference on Computer Vision and Pattern Recognition. Salt Lake City, 2018. 2724–2732
32 Zhang J, Ding Z W, Li W Q, et al. Importance weighted adversarial nets for partial domain adaptation. In: Proceedings of the IEEE Conference on Computer Vision and Pattern Recognition. Salt Lake City, 2018. 8156–8164
33 Li W H, Chen Z Y, He G. A novel weighted adversarial transfer network for partial domain fault diagnosis of machinery. IEEE Trans Ind Inf, 2020, 17: 1753–1762
34 Li X, Zhang W. Deep learning-based partial domain adaptation method on intelligent machinery fault diagnostics. IEEE Trans Ind Electron, 2020, 68: 4351–4361
35 Deng Y F, Huang D L, Du S C, et al. A double-layer attention based adversarial network for partial transfer learning in machinery fault diagnosis. Comput Industry, 2021, 127: 103399
36 Liu Z H, Lu B L, Wei H L, et al. A stacked auto-encoder based partial adversarial domain adaptation model for intelligent fault diagnosis of rotating machines. IEEE Trans Ind Inf, 2021, 17: 6798–6809
37 Li X, Zhang W, Ma H, et al. Partial transfer learning in machinery cross-domain fault diagnostics using class-weighted adversarial networks. Neural Networks, 2020, 129: 313–322
38 Moaveni S. Finite Element Analysis Theory and Application with ANSYS, 3rd ed. New Jersey: Prentice Hall, 2007
39 Zapico-Valle J L, Alonso-Camblor R, González-Martínez M P, et al. A new method for finite element model updating in structural dynamics. Mech Syst Signal Process, 2010, 24: 2137–2159

40 Wang K F, Gou C, Duan Y J, et al. Generative adversarial networks: The state of the art and beyond. Acta Autom Sin, 2017, 43: 321–332
41 Grandvalet Y, Bengio Y. Semi-supervised learning by entropy minimization. Adv Neural Inf Process Syst, 2004, 17
42 Ganin Y, Lempitsky V. Unsupervised domain adaptation by backpropagation. 2015, arXiv: 1409.7495v2
43 Smith W A, Randall R B. Rolling element bearing diagnostics using the Case Western Reserve University data: A benchmark study. Mech Syst Signal Process, 2015, 64-65: 100–131
44 Song W L, Xiang J W, Zhong Y T. A simulation model based fault diagnosis method for bearings. J Intell Fuzzy Syst, 2018, 34: 3857–3867
45 Biswas S K, Milanfar P. One shot detection with laplacian object and fast matrix cosine similarity. IEEE Trans Pattern Anal Mach Intell, 2016, 38: 546–562
46 Kingma D P, Ba J. Adam: A method for stochastic optimization. 2017, arXiv: 1412.6980v9
47 Verstraete D B, Droguett E L, Meruane V, et al. Deep semi-supervised generative adversarial fault diagnostics of rolling element bearings. Struct Health Monit, 2020, 19: 390–411
48 Van der Maaten L, Hinton G. Visualizing data using t-SNE. J Mach Learn Res, 2008, 9: 2579–2605